Dye Sensitized TiO$_2$ and ZnO Charge Transport Layers for Efficient Planar Perovskite Solar Cells: Experimental and DFT Insights

RIHAB CHOUK,[1,2] DJEDJIGA HAOUANOH,[3] CHADLIA AGUIR,[2,4]
MANEL BERGAOUI,[1,2] MAHDIA TOUBANE,[3] FAYÇAL BENSOUICI,[3]
RAZIKA TALA-IGHIL,[3] ALESSANDRO ERTO,[5]
and MOHAMED KHALFAOUI [1,2,6]

1.—Research Group in Materials Sciences, Microelectronics and Nanotechnologies, Department of Technology, Higher Institute of Computer Sciences and Mathematics of Monastir, University of Monastir, 5000 Monastir, Tunisia. 2.—Laboratory of Physical Chemistry of Materials, Department of Physics, Faculty of Sciences, University of Monastir, 5000 Monastir, Tunisia. 3.—Department of Physics, URMPE Unit, UMBB University, 35000 Boumerdes, Algeria. 4.—High School of Health Sciences and Techniques of Monastir, University of Monastir, 5000 Monastir, Tunisia. 5.—Dipartimento di Ingegneria Chimica, dei Materiali e della Produzione Industriale, Università degli Studi di Napoli Federico II, Piazzale Vincenzo Tecchio 80, 80125 Naples, Italy. 6.—e-mail: mohamed.khalfaoui@isimm.rnu.tn

In this work, the efficiency improvement of planar perovskite solar cells by the introduction of modified electron transport layers (ETLs) is investigated. To this aim, a cobalt complex dye as sensitizer for TiO$_2$, based on Schiff base ligand (Co-NG), and a ZnO layer were prepared by the sol gel method and are tested. The electrodes and the complex are characterized by x-ray diffraction, TGA/DSC and UV–Vis spectroscopy. The photo-physical properties of Co-NG complex investigated at the molecular level show that the dye exhibits good optical behavior with two maxima around 415 nm and 604 nm and a high molar extinction coefficient equal to $27.5 \times 10^3 \text{ M}^{-1} \text{ cm}^{-1}$. The influence of sensitization on the optical properties of the ETLs is tested and strong interactions between the dye and the ETLs are found. As a result, the solar cell performances of TiO$_2$/Co-NG and ZnO/Co-NG exhibit a significant efficiency increase equal to 18.94% and 16.32%, respectively, compared to the reference solar cells.

Key words: Perovskite solar cells, DFT calculations, sensitized ETLs, spectroscopic characterization, electrical stimulation

INTRODUCTION

In recent years, organic–inorganic perovskite solar cells (PSCs) have attracted great interest due to their low-cost fabrication process and their photo-physical properties that allow achieving a high power conversion efficiency, which presently exceeds 22.7%.[1,2] In this context, many strategies have been proposed to further improve the efficiency of PSCs. One of the most important aspects that influence the efficiency of PSCs is the properties of the electron transporting layers (ETLs), which can be built with interesting materials such as TiO$_2$ and ZnO layers. In fact, many researchers have proved that a more efficient charge transfer takes place at the interface of ETL/perovskite with respect to that of the classic perovskite/hole transport layer (HTL), thus playing a crucial role for the further improvement of device performance and stability.[2,3] In this context, several studies have been specifically focused on improving the properties at the interface between the electron transport materials (e.g., TiO$_2$

Dye Sensitized TiO$_2$ and ZnO Charge Transport Layers for Efficient Planar Perovskite Solar
Cells: Experimental and DFT Insights

1397

and ZnO) and the perovskite layers.[4–6] As an example, the work of Kim et al.[7] investigated the effect of Nb-doped TiO$_2$ on the electronic structure and photovoltaic properties of PSCs. In this study, remarkable modifications of the electronic band structures and surface states of the electron transport layer were found. Similar results were achieved by other researchers, which proved that TiO$_2$ and ZnO superficial modifications are effective in enhancing the charge collection and the electrical properties of PSCs.[8–11]

Additionally, an innovative engineering approach has been proposed by introducing the original concept of dye-sensitization, so to optimize the properties at the perovskite/ETLs interface and aimed at developing more efficient PSCs. According to a previous work,[12–15] the insertion of a dye proved to determine an efficient improvement of the final device properties, by reducing charges recombination, facilitating charge transfer, minimizing the energy level and improving the perovskite crystallization. In turn, these effects alter in a beneficial manner the electron collection rate, thus directly affecting the device efficiency. Some examples of such an approach include the recent publications of Wang et al.[16] and Li et al.[17] that showed an enhancement in the efficiency from 14% (obtained in a reference cell) to 16.2% and an improvement of the stability by employing dye-sensitized nickel oxide (NiO$_x$). Simultaneously, Balis et al.[18] proved that the use of porphyrin-modified TiO$_2$ as ETL significantly improves the performances and increases the stability of PSC using non-modified TiO$_2$, with an efficiency enhancement from 15.01% to 16.87%. This work provides significant insights to ameliorate TiO$_2$ and ZnO material properties and interfacial passivation (TiO$_2$/Perovskite and ZnO/Perovskite) by dye modification of ETLs for a better exploiting of advanced perovskite solar cell technology.

Due to their interesting properties such as the high molar extinction coefficient, Schiff base complexes derived from ninhydrin and α-amino acid have attracted considerable attention in optoelectronic devices, such as organic light emitting diodes and solar cells.[19–21] In fact, in our previous work a detailed structural and optical investigation on cobalt schiff base complex has been carried out to prove their good injection properties in dye sensitized solar cells. From these interesting results, we have deduced that this complex can work effectively in cooperation with ETLs which makes it also a good candidate for perovskite solar cells.

Thus, in the present work, we report the dye-modification of titanium dioxide and Zinc dioxide as efficient electron transport layers for planar PSC. More specifically, we use a Schiff base complex derived from ninhydrin and glycine (Co-NG) as sensitizer in order to improve the electron transfer, the efficiency and the stability of PSC. The synthesis procedure and the structural, optical and electronic properties of Co-NG complex dye were accurately studied. In addition, to provide further insights into the properties of these materials at the molecular level, DFT and TD-DFT calculations were carried out. The effect of Co-NG dye sensitization of TiO$_2$ and ZnO layers on the optical properties was assessed. The prepared samples were characterized using x-ray diffraction, TGA/DSC and UV–Vis spectroscopy. All these properties were evaluated in the same framework in order to determine the potential applications as ETLs in PSCs. Finally, a numerical simulation using SCAPS software was performed in order to investigate the impact of TiO$_2$/Co-NG and ZnO/Co-NG films on some electrical properties, such as open-circuit voltage, short-circuit current and efficiency for a conventional PSC.

EXPERIMENTAL SECTION

Synthesis of Dye

The general protocol of synthesis of Schiff base cobalt complex was described in detail in our previous published work.[22] The general process was also described elsewhere.[23,24] The chemical structure of the Schiff base cobalt complex is illustrated in Fig. 1.

Films Preparation of TiO$_2$ and ZnO

A simple and cost-effective sol–gel dip-coating method was used for the deposition of TiO$_2$ and ZnO films. The TiO$_2$ and ZnO films were performed by a dip coater onto glass substrate using a withdrawal of 1 mm/s and with 1 min and 30 s immersion time for TiO$_2$ and ZnO, respectively. After each dipping, the samples are pre-heated at 400°C for 10 min to eliminate some organic compounds and avoid the cracks of films.[26,27] Finally, the materials were annealed in air for 1 h at 450°C. Note that the layer thickness of TiO$_2$ and ZnO films was indirectly controlled by the dipping number.

For TiO$_2$ departure solution, titanium (IV) n-propoxide (Ti (OCH$_2$CH$_2$CH$_3$)$_4$) was dissolved in a
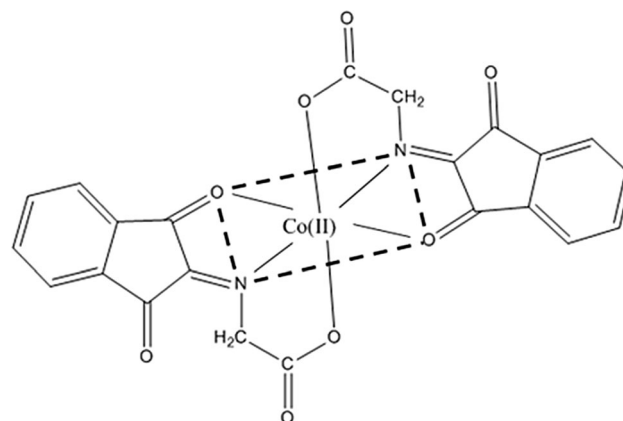

Fig. 1. Chemical structure of Co-NG complex dye.[25] Only data was used from cited reference.

solution containing ethanol (C_2H_6O), water and nitric acid (HNO_3). The adopted molar ratio are 1.00/0.55/0.33/21.18 for [Ti]/[H_2O]/[HNO_3]/ethanol, respectively. The solution is stirred for 1 h at room temperature under atmospheric pressure. As a result, the final solution becomes transparent and light-yellow colored.

The precursor solution of ZnO was prepared using Zinc acetate dehydrate (Zn ($CH_3COO)_2$. $2H_2O$), ethanol (C_2H_6O) and diethanolamine (HN (CH_2CH_2 $OH)_2$) as starting precursor, solvent and stabilizer, respectively. In the sol, Zn^{2+} concentrations were chosen as 0.4 M. Firstly, zinc acetate was dissolved in ethanol at room temperature and the resulting mixture was stirred at 60°C for 1 h. Then, diethanolamine was added drop-by drop into the solution. The diethanolamine molar ratio to Zn^{2+} was maintained at 1.0. Finally, a transparent and homogeneous result was obtained.

Characterization

Physical Analyses

Molar conductivity of 10^{-3} M solutions of the complex in DMSO was measured using a conductivity meter ORION model 150 of 0.6 cell constant. The melting point of the Co (II) complex was recorded using IA 9200 digital melting point apparatus.

X-ray Powder Diffraction

Powder x-ray diffraction analysis was performed by a Rigaku Ultima IV diffractometer instrument with Cu–Kα radiation (wavelength 0.154 nm) operating at 40 kV and 45 mA. Measurements were scanned for diffraction angles (2θ) ranging from 5° to 118° with a step size of 0.01° and a time per step of 1 min.

Thermal Analyses

Thermal measurements were carried out in the temperature range 25–800°C for differential scanning colorimetric (DSC) and thermo-gravimetric analysis (TGA) using STA 409 pc Luxx NETZSCH.

UV–Vis Spectroscopy

The UV–visible absorption spectra were recorded usinga LI-2802 double beam spectrophotometer (Lasany, Haryana, India) in the 200–1100 nm region.

COMPUTATIONAL METHODS

The molecular structures of a Co-NG complex were optimized using Gaussian 09 software.[28] Then, the calculations were carried out at the density functional Theory (DFT) level as detailed in our previous paper.[22] Furthermore, to get deeper insight the optical and electronic properties, time dependent density functional theory (TD-DFT) calculations were adopted. Using TD-DFT calculation, we can estimate interesting properties such as the highest occupied molecular orbital (HOMO), the lowest unoccupied molecular orbital (LUMO) and the gap energy (E_g). Indeed, many researchers have proved that the theoretical TD-DFT/B3LYP levels are good and reliable to reproduce the experimental data.[29–31] The 20 lowest singlet electronic transitions were calculated and processed with the GaussSum software package.[32]

Additionally, in order to investigate the impact of the introduction of sensitized TiO_2 and ZnO electrodes in Perovskite Solar Cells devices, one-dimensional device simulations were carried out with the software SCAPS, developed at the University of Gent.[33] It is an efficient solar cell simulation tool to analyze the transport behavior and the description of recombination in optoelectronic device structures by using the continuity and Poisson's equations approach. Recently, many researchers have confirmed the validity of SCAPS tool simulation by comparing the simulation results with the device performances deriving from real experimental characterization.[34] However, for that purpose, it would be opportune to design devices that can be helpful to guide and experimentally support the subsequent fabrication process.

RESULTS AND DISCUSSION

Physical Properties

Some physical properties of the investigation Co-NG metal complex are shown in Table I. The complex of Co (II) is dark green colored,with powdered solids, which decomposes above 350°C. It is stable to atmospheric conditions at room temperature and insoluble in water and most organic solvents but soluble in solvent of high dielectric strength like DMSO (giving a light blue color solution).

The Co(II) complex shows only one spot on the TLC indicating the complex formed was pure. This is also confirmed by the sharp melting point of the complex. Furthermore, the complex is subjected to chloride analysis by fusion test and precipitation as AgCl.[35] The result indicates the absence of chloride in the complex.
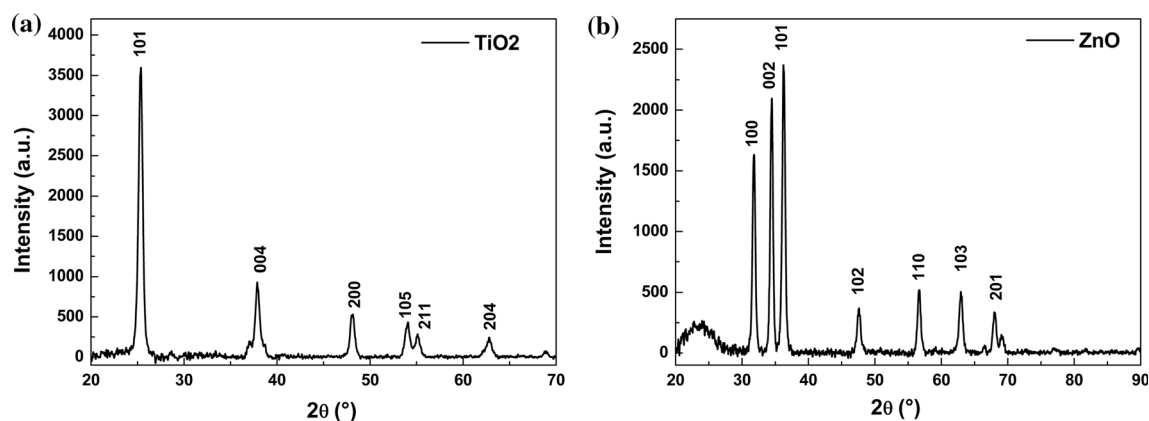
The electrical conductivity measurements of Co-NG complex in DMSO give Λ_M value of 28 Ω^{-1} cm^2 mol^{-1} and confirm that it is neutral and no electrolyte.[25]

Structural Properties

The x-ray diffraction (XRD) patterns of TiO_2, ZnO films are shown in Fig. 2. Table II presents some structural parameters such as the average crystallite size, the lattice parameters, the microstrain and the Rietveld refined data. A low value of the fitting parameter χ^2 was observed, which justifies the good refinement quality.

Dye Sensitized TiO_2 and ZnO Charge Transport Layers for Efficient Planar Perovskite Solar Cells: Experimental and DFT Insights

1399

Table I. Physical characteristics of the Co-NG complex

Yield%	Color and appearance	Decomposition temperature (°C)	Melting point (°C)	Molar conductance (Ω^{-1} cm^2 mol^{-1})
52	Dark green, powder	> 350	330	28

Fig. 2. XRD patterns of (a) TiO_2 and (b) ZnO.

Table II. Structural and microstructural parameters of the synthesized ZnO and TiO_2

	Crystallite size (nm)	Microstrain (%)	Lattice parameters (Å)	Rwp (%)	Rp (%)	Re (%)	S	χ^2
ZnO	19.3	0.64	3.25 5.210	9.59	6.20	6.06	1.58	2.50
TiO_2	18.8	0.93	3.78 9.51	17.88	11.45	14.51	1.11	1.24

The crystallite size was determined from the diffraction peak broadening, by employing the Scherrer's equation[36] as follows:

$$D = \frac{0.94\lambda}{\cos(\theta)\beta},\qquad(1)$$

where λ is the wavelength of the x-ray beam, θ is the incidence angle and β is the full width at half maximum (FWHM) of the diffraction peak.

All the observed diffraction peaks shown in Fig. 2a were indexed within anatase TiO_2 phase with a preferred orientation along the [001] plane. These results are in agreement with the JCPDS Card No. 21-1272;[37] furthermore, a crystallite size of 18.8 nm was measured.

In the case of ZnO film (Fig. 2b), it can be clearly observed that it crystallizes as Zincite-type structure with a crystallite size equal to 19.3 nm. Our results are in agreement with those retrieved in previous works[38,39] and the diffraction peaks are preferentially oriented along the (101) plane.

Furthermore, the crystalline structure of Co-NG, published in our previous work,[22] reveals that this complex belongs to a triclinic system with the following unit cell parameters: a = 17.4315 Å, b = 16.1949 Å, c = 15.0722 Å, α = 83.2199°, β = 111.978°, χ = 132.756°.

Thermal Analyses of Co-NG Dye

The simultaneous TG/DSC analysis of the Co (II) metal complexes was studied from ambient temperature to 800°C under a nitrogen atmosphere (Fig. 3). The TG curve of the Co (II) complexes exhibited no mass loss up to 325°C, indicating the absence of coordinated water and the high thermal stability of the complexes.[40]

The TG curve of the Co (II) complex shows also a two-steps decomposition pattern. The first step, from 325°C to 360°C with a mass loss of 39.09%, is accompanied by an endothermic peak with T_{max} = 355°C on the DTA curve, that can be likely attributed to the removal of the non-coordinated
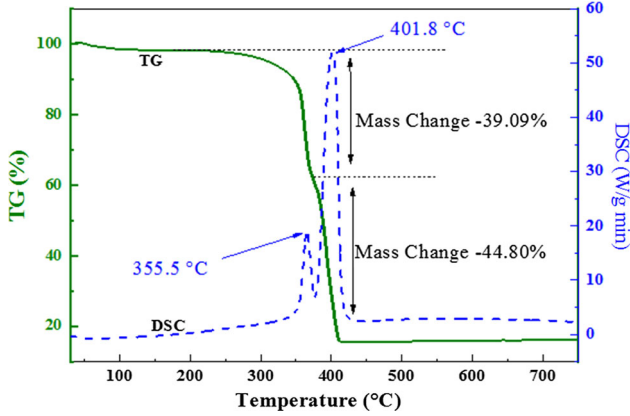
Fig. 3. TGA-DSC spectra analysis of Co-NG Dye.

part of the ligand. The second step, from 365°C to 410°C with mass loss of 44.80%, corresponds to the decomposition of the coordinated part of the ligand. For this step, a broad endothermic peak in the DTA was observed.[41] These results are in good agreement with those reported in a previous work of Rao et al.[42]

Co-NG Sensitized TiO₂ and ZnO Electrodes

According to our previous published results[22] about HOMO–LUMO transitions, the carboxylate groups can act as anchors to the TiO₂ semiconductor surface, which favor the electron injection from the dye excited state into the semiconductor conduction band.[43] It is interesting to estimate some key parameters of solar cell based on the studied complex. In fact, for an efficient electron injection, suitably aligned energy levels are required. For this, the LUMO of Co-NG needs to be higher than the conduction band (CB) of TiO₂ and ZnO electrodes.

Indeed, the conversion efficiency (η) of solar energy to electricity of the solar cell devices can be obtained from the following equation:

$$\eta = \frac{J_{SC} V_{OC} FF}{P_{in}}, \tag{2}$$

where J_{SC} is the short-circuit current density, V_{OC} is the open circuit photo voltage, FF is the fill factor and P_{in} represents the light intensity.

Correspondingly, J_{SC} can be expressed as:[44]

$$J_{SC} = \int LHE(\lambda) \cdot \emptyset_{inj} \cdot \eta_{coll} d\lambda \tag{3}$$

with LHE is the light harvesting efficiency of the dye, $\emptyset_{inj}$ represents the quantum yield of electron injection and η_{coll} is the electron collection efficiency.

These parameters should be as large as possible to have a good efficiency. For this, we have calculated the electron injection (transfer) potential, $\emptyset_{inj}$, of the dye as follows:

$$\emptyset_{inj} = E_{ox}^{dye*} - E_{CB}^{SC} \tag{4}$$

in which E_{ox}^{dye*} is the oxidation potential of the Co-NG dye in the excited state and E_{CB}^{SC} is the conduction band of the TiO₂ and ZnO layers, which has an experimental value equal to 4.00 eV. A negative value of $\emptyset_{inj}$ (− 0.29 eV) was found, revealing that the excited states of Co-NG lie above the TiO₂ and ZnO and, hence, favoring the electron injection into the conduction band. Additionally, the light harvesting efficiency (LHE) was estimated according to Eq. 3:

$$LHE = 1 - 10^{-f}, \tag{5}$$

where f is the dye's oscillator strength corresponding to the maximum wavelength. This parameter is a dimensionless quantity that expresses the probability of absorption in transitions between energy levels of the molecule. It can be thought of as the ratio between the quantum mechanical transition rate and the classical absorption of a single electron oscillator with the same frequency as the transition.

A good light harvesting efficiency equal to 0.75 was obtained. This is an important parameter for the assessment of the overall solar cell device performances since the short-circuit photocurrent density (J_{sc}) largely depends on the light-harvesting ability, which is also directly related to the optical absorption spectrum. Hence, a good power conversion efficiency is expected.

Based on the above results, the effect of sensitization on the optical and electronic properties of TiO₂ and ZnO thin films was investigated. The prepared substrates were immersed in a solution of Co-NG dye (0.3 mM) in THF solvent. The changes in electrodes color are visible also by the naked eye.

The UV–visible absorption spectra of the electrodes before and after the modification were recorded (Fig. 4). This was very important to confirm the deposition of Co-NG dye on TiO₂ and ZnO ETLs.

The dye anchoring into the ETLs resulted in a decrease of the TiO₂ and ZnO transmittance. From Fig. 4, it can be noticed the appearance of a Q band at 625 nm. Compared to the absorption spectrum of Co-NG dye, this Q band was redshifted of 14 nm. This indicates the strong intermolecular interaction between Co-NG dye and ZnO surface. The same result was observed for TiO₂/Co-NG film, which showed a Q band redshift of 11 nm. In fact, as it can be seen, the spectrum shows strong visible absorption due to the electron coupling derived from the interaction between the dye molecules and TiO₂.

From the above study, we can deduce that the sensitization of ZnO and TiO₂ ETLs have affected the optical properties of TiO₂ and ZnO and, consequently their band gap. This can improve the absorption of the incident photons and decrease the barrier height between Fluorine doped tin oxide (FTO) and the sensitized TiO₂ and ZnO layers. Moreover, the interaction between the ETLs and Co-NG dye can offer additional stability and
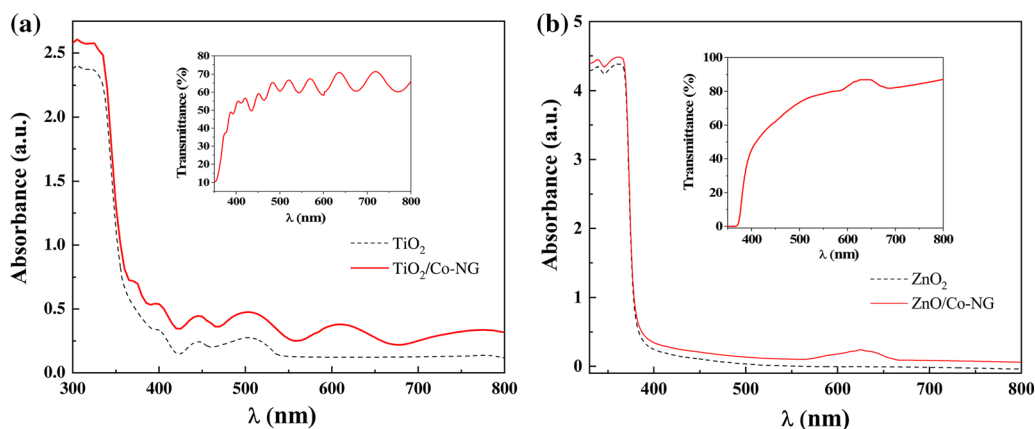
Dye Sensitized TiO₂ and ZnO Charge Transport Layers for Efficient Planar Perovskite Solar Cells: Experimental and DFT Insights

1401

Fig. 4. Absorption spectra of (a) TiO₂ and (b) ZnO films before and after Co-NG sensitization.
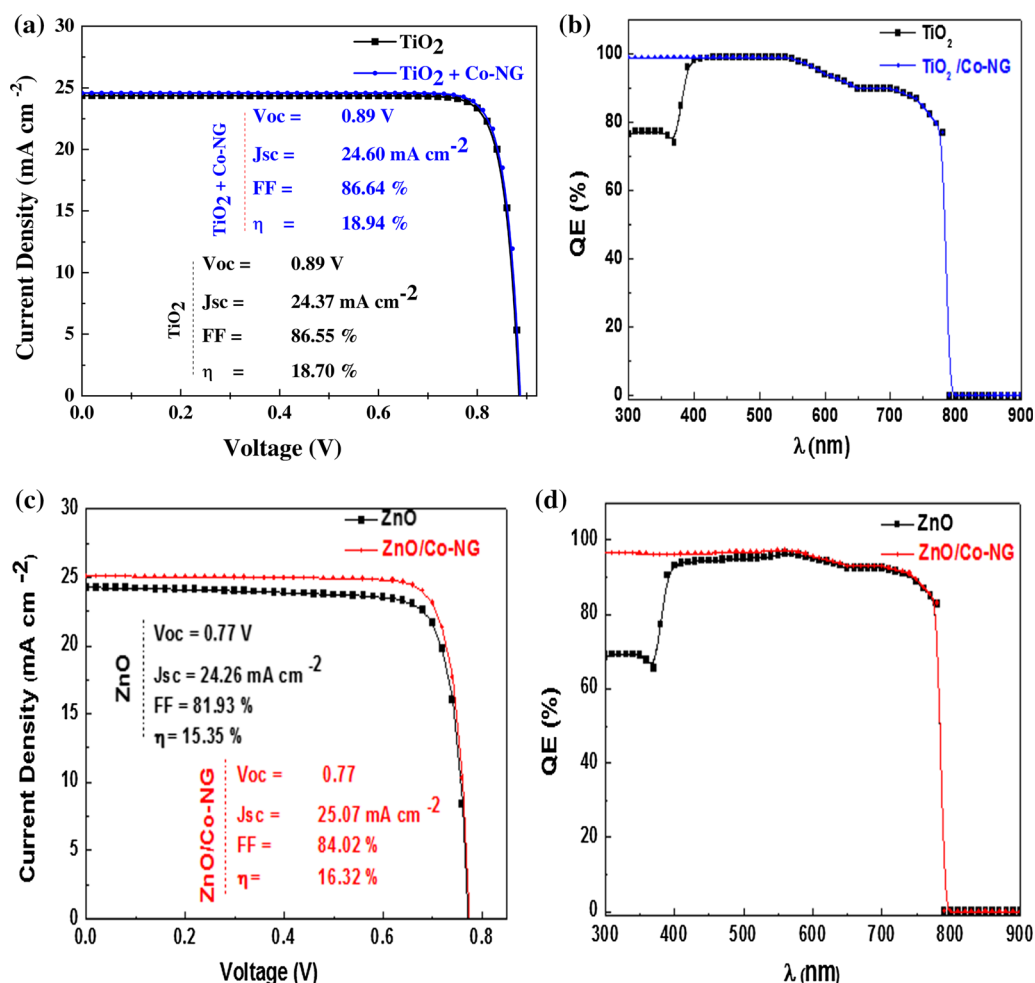

Fig. 5. I–V current density and quantum efficiency characteristics of perovskite solar cells based on (a) TiO₂ and (b) modified TiO₂ and (c) ZnO and (d) modified ZnO.

promote the perovskite layer degradation; hence, it is evident that the sensitization brought some important beneficial effects. Consequently, it is expected to obtain a perovskite solar cell with enhanced performance.

Photovoltaic Performances

First, as a baseline to verify the effectiveness of our approach, the standard sandwiched planar perovskite solar cells in FTO/TiO₂/MAPbI3/spiro-OMeTAD/Ag and FTO/ZnO/MAPbI₃/spiro-

Table III. Simulated values of device performance parameters

Device	V_{oc} (V)	J_{sc} (mA/cm^2)	FF (%)	η (%)
FTO/TiO$_2$/MAPbI$_3$/Spiro-OMeTAD/Ag	0.89	24.38	86.55	18.70
FTO/TiO$_2$/Co-NG/MAPbI$_3$/Spiro-OMeTAD/Ag	0.89	24.60	86.64	18.94
FTO/ZnO/MAPbI$_3$/Spiro-OMeTAD/Ag	0.77	24.26	81.93	15.35
FTO/ZnO/Co-NG/MAPbI$_3$/Spiro-OMeTAD/Ag	0.78	25.07	84.02	16.32

OMeTAD/Ag configurations were simulated using SCAPS software. Here, in both the configurations, TiO$_2$ and ZnO films act as blocking layers, the spiro-OMeTAD is a p-type hole transportation layer and MAPbI$_3$ is the absorber perovskite. The hole material of spiro-OMeTAD is dopant-free. Moreover, the FTO is the transparent conductive oxide and Ag serves as metal back contact.

Note that the SCAPS simulation enables the material properties definition such as the gap, the acceptor density, the donor density, the band gap energy, the electron affinity, the relative dielectric permittivity, the mobility of electrons, the mobility of hole and the absorption spectrum for each film. In addition, we must introduce the barrier height at the back and front contacts, which are estimated by comparing the work function of FTO and Ag electrodes with the HOMO and LUMO levels of the interfacial layers. The materials baseline parameters were carefully chosen from previously reported experimental works available in the literature.[45,46]

The obtained I-V curves and Quantum efficiency characteristics of the reference solar cells are shown in Fig. 5 while in Table III we summarize the simulated values of device performance parameters, such as short-circuit current density (J_{sc}), open-circuit voltage (V_{oc}), fill factor (FF) and efficiency (η).

An efficiency of 18.70% was obtained for the FTO/TiO$_2$ (30 nm)/MAPbI$_3$ (300 nm)/spiro-OMeTAD (150 nm)/Ag solar cell, closely reproducing the experimental results reported by Ahn et al. and the simulated one reported by Wang et al.[47] At the same time, the simulation results of FTO/ZnO/MAPbI$_3$/spiro-OMeTAD/Ag solar cell resulted in good agreement with those reported in a previous work of Lin et al.[48] Since the simulation gave accurate results, it indicated the reliability of our approach. For this reason, we have used these standard solar cell configurations to study the effect of sensitized TiO$_2$ and ZnO ETLs on the photovoltaic parameters. The schematic proposed architectures are shown in Fig. 6 and the input parameters of TiO$_2$/Co-NG and ZnO/Co-NG films were retrieved from our theoretical and experimental results.

The device performance with Co-NG sensitized ZnO and TiO$_2$ are depicted in Fig. 6. Importantly, an enhanced efficiency of 18.94% was reached using Co-NG/TiO$_2$ and 16.32% using Co-NG/ZnO, which represent a 1.2% and 6% improvement, respectively, compared to the reference devices. The key

Fig. 6. Energy level diagram of the studied perovskite solar cells.

parameter of this enhancement is the short-circuit current density, J_{sc}, increase. Meanwhile, we make an estimation of the J_{sc} improvement from the transmittance spectrum since the sensitization of TiO$_2$ and ZnO enhances the light trapping. Thus, the electrodes would absorb more photons with longer wavelength, promoting the decrease in gap energy. Consequently, the barrier height between FTO and the sensitized TiO$_2$ and ZnO layers decreases and a barrier free electron extraction is expected between the sensitized ETLs and perovskite. Our results were further supported by the increase in quantum efficiency. Importantly, we can notice that the power conversion efficiency increases up to the highest point of 98.9% for sensitized TiO$_2$ and 96.1% for sensitized ZnO at 300–350 nm. This is due to the electrode's sensitization, which makes the TiO$_2$ and ZnO layers sufficient to absorb most of the incident photons. Furthermore, the higher conversion efficiency of the modified cell can be ascribed to the good photo-induced electron injection of Co-NG, which leads to an enhanced electron collection as we previously discussed.

CONCLUSION

In the current study, we have proposed and demonstrated the suitability of dye sensitization of TiO$_2$ and ZnO ETL layers for high efficiency energy conversion. For this goal, a cobalt complex dye as sensitizer for TiO$_2$ and ZnO layers was prepared and characterized. We show within this paper the impact of the sensitization on the optical properties of the electron transporting layers. The Co-NG dye

Dye Sensitized TiO$_2$ and ZnO Charge Transport Layers for Efficient Planar Perovskite Solar Cells: Experimental and DFT Insights

1403

modification of TiO$_2$ film enhanced the performance of the overall device from 18.70% to 18.94%. Similarly, an enhancement from 15.35% to 16.32% using ZnO/Co-NG was obtained by using SCAPS software. Thanks to the sensitization procedure, the efficiency enhancement was the result of a large increase in J_{sc}, which originates from the increased electron transfer and the enhanced absorption of the incident photons.

ACKNOWLEDGMENTS

REFERENCES

1. J.H. Noh, S.H. Im, J.H. Heo, T.N. Mandal, and S.I. Seok, *Nano Lett.* 13, 1764 (2013).
2. J. You, L. Meng, T.-B. Song, T.-F. Guo, Y.M. Yang, W.-H. Chang, Z. Hong, H. Chen, H. Zhou, and Q. Chen, *Nat. Nanotechnol.* 11, 75 (2016).
3. T. Singh, S. Öz, A. Sasinska, R. Frohnhoven, S. Mathur, and T. Miyasaka, *Adv. Funct. Mater.* 28, 1706287 (2018).
4. S. Li, P. Zhang, Y. Wang, H. Sarvari, D. Liu, J. Wu, Y. Yang, Z. Wang, and Z.D. Chen, *Nano Res.* 10, 1092 (2017).
5. H. Xie, X. Yin, J. Liu, Y. Guo, P. Chen, W. Que, G. Wang, and B. Gao, *Appl. Surf. Sci.* 464, 700 (2019).
6. M. Zhong, L. Chai, and Y. Wang, *Appl. Surf. Sci.* 464, 301 (2019).
7. D.H. Kim, G.S. Han, W.M. Seong, J.W. Lee, B.J. Kim, N.G. Park, K.S. Hong, S. Lee, and H.S. Jung, *ChemSusChem* 8, 2392 (2015).
8. A.N. Cho and N.G. Park, *ChemSusChem* 10, 3687 (2017).
9. Y. Li, Y. Zhao, Q. Chen, Y. Yang, Y. Liu, Z. Hong, Z. Liu, Y.-T. Hsieh, L. Meng, and Y. Li, *J. Am. Chem. Soc.* 137, 15540 (2015).
10. K. Mahmood, B.S. Swain, and A. Amassian, *Adv. Energy Mater.* 5, 1500568 (2015).
11. D.-Y. Son, J.-H. Im, H.-S. Kim, and N.-G. Park, *J. Phys. Chem. C* 118, 16567 (2014).
12. Y. Bai, H. Chen, S. Xiao, Q. Xue, T. Zhang, Z. Zhu, Q. Li, C. Hu, Y. Yang, and Z. Hu, *Adv. Funct. Mater.* 26, 2950 (2016).
13. N. Balis, A.A. Zaky, D. Perganti, A. Kaltzoglou, L. Sygellou, F. Katsaros, T. Stergiopoulos, A.G. Kontos, and P. Falaras, *ACS Appl. Energy Mater.* 1, 6161 (2018).
14. A.N. Gusev, M.A. Kiskin, E.V. Braga, M. Chapran, G. Wiosna-Salyga, G.V. Baryshnikov, V.A. Minaeva, B.F. Minaev, K. Ivaniuk, and P. Stakhira, *J. Phys. Chem. C* 123, 11850 (2019).
15. Q. Xue, Y. Bai, M. Liu, R. Xia, Z. Hu, Z. Chen, X.F. Jiang, F. Huang, S. Yang, and Y. Matsuo, *Adv. Energy Mater.* 7, 1602333 (2017).
16. Q. Wang, C. Chueh, T. Zhao, J. Cheng, M. Eslamian, W. Choy, and A. Jen, *ChemSusChem* 10, 3794 (2017).
17. X. Li, X. Zhao, F. Hao, X. Yin, Z. Yao, Y. Zhou, H. Shen, and H. Lin, *ACS Appl. Mater. Interfaces* 10, 17861 (2018).
18. N. Balis, A. Verykios, A. Soultati, V. Constantoudis, M. Papadakis, F. Kournoutas, C. Drivas, M.-C. Skoulikidou, S. Gardelis, and M. Fakis, *ACS Appl. Energy Mater.* 1, 3216 (2018).
19. I.M. Alaoui and E.R. Menzel, *Forensic Sci. Int.* 77, 3 (1996).
20. P. Davies, H. Kobus, M. Taylor, and K. Wainwright, *J. Forensic Sci.* 40, 565 (1995).
21. E. Menzel and K. Mitchell, *J. Forensic Sci.* 35, 35 (1990).
22. R. Chouk, C. Aguir, D. Haouanoh, M. Bergaoui, R. Tala-Ighil, E. Stathatos, and M. Khalfaoui, *J. Mol. Struct.* 1196, 676 (2019).
23. Z. Khan, S. Ali, D. Gupta, and A. Khan, *Indian J. Chem.* 35A, 320 (1996).
24. Z. Khan, A. Hashmi, T.A. Khan, and M. Haq, *Int. J. Chem. Kinet.* 28, 893 (1996).
25. M.G. Derebe, V. Raju, and N. Retta, *Bull. Chem. Soc. Ethiop.* 16, 53 (2002).
26. F. Bensouici, T. Souier, A. Dakhel, A. Iratni, R. Tala-Ighil, and M. Bououdina, *Superlattices Microstruct.* 85, 255 (2015).
27. M. Toubane, R. Tala-Ighil, F. Bensouici, M. Bououdina, W. Cai, S. Liu, M. Souier, and A. Iratni, *Ceram. Int.* 42, 9673 (2016).
28. M.J. Frisch, G.W. Trucks, H.B. Schlegel, G.E. Scuseria, M.A. Robb, J.R. Cheeseman, G. Scalmani, V. Barone, B. Mennucci, G.A. Petersson, H. Nakatsuji, M. Caricato, X. Li, H.P. Hratchian, A.F. Izmaylov, J. Bloino, G. Zheng, J.L. Sonnenberg, M. Hada, M. Ehara, K. Toyota, R. Fukuda, J. Hasegawa, M. Ishida, T. Nakajima, Y. Honda, O. Kitao, H. Nakai, T. Vreven, J.A. Montgomery, Jr., J.E. Peralta, F. Ogliaro, M. Bearpark, J.J. Heyd, E. Brothers, K.N. Kudin, V.N. Staroverov, R. Kobayashi, J. Normand, K. Raghavachari, A. Rendell, J.C. Burant, S.S. Iyengar, J. Tomasi, M. Cossi, N. Rega, J.M. Millam, M. Klene, J.E. Knox, J.B. Cross, V. Bakken, C. Adamo, J. Jaramillo, R. Gomperts, R.E. Stratmann, O. Yazyev, A.J. Austin, R. Cammi, C. Pomelli, J.W. Ochterski, R.L. Martin, K. Morokuma, V.G. Zakrzewski, G.A. Voth, P. Salvador, J.J. Dannenberg, S. Dapprich, A.D. Daniels, Ö. Farkas, J.B. Foresman, J.V. Ortiz, J. Cioslowski, and D.J. Fox, Gaussian 09 (Gaussian, Inc.: Wallingford, CT, 2009).
29. R. Chouk, M. Bergaoui, N. Jaballah, M. Majdoub, and M. Khalfaoui, *J. Mol. Liquids* 284, 193 (2019).
30. A. Irfan, A.G. Al-Sehemi, A.R. Chaudhry, and S. Muhammad, *J. King Saud Univ. Sci.* 30, 75 (2018).
31. A. Irfan, A. Kalam, A.R. Chaudhry, A.G. Al-Sehemi, and S. Muhammad, *Optik* 132, 101 (2017).
32. N.M. O'boyle, A.L. Tenderholt, and K.M. Langner, *J. Comput. Chem.* 29, 839 (2008).
33. M. Burgelman, P. Nollet, and S. Degrave, *Thin Solid Films* 361, 527 (2000).
34. K. Tan, P. Lin, G. Wang, Y. Liu, Z. Xu, and Y. Lin, *Solid State Electron.* 126, 75 (2016).
35. J. Basset, R. Denny, G. Jeffery, and J. Mendham, *Appl. Clay Sci.* 19, 13 (1986).
36. A. Stokes and A. Wilson, *Proc. Phys. Soc.* 56, 174 (1944).
37. H.E. Swanson and E. Tatge, *J. Res. Natl. Bur. Stand.* 46, 318 (1951).
38. S. Bouhouche, F. Bensouici, M. Toubane, A. Azizi, A. Otmani, K. Chebout, F. Kezzoula, R. Tala-Ighil, and M. Bououdina, *Mater. Res. Express* 5, 056407 (2018).
39. M. Toubane, R. Tala-Ighil, F. Bensouici, M. Bououdina, M. Souier, S. Liu, W. Cai, and A. Iratni, *Mater. Res. Express* 4, 035023 (2017).
40. D. Dash, A. Panda, P. Jena, S. Patjoshi, and A. Mohapatra, *J. Indian Chem. Soc.* 79, 48 (2002).
41. A.S. Munde, A.N. Jagdale, S.M. Jadhav, and T.K. Chondhekar, *J. Serb. Chem. Soc.* 75, 349 (2010).
42. N.K. Rao and M.R. Reddy, *Biol. Met.* 3, 19 (1990).
43. C.I. Oprea, P. Panait, J. Lungu, D. Stamate, A. Dumbravă, F. Cimpoesu, and M.A. Gîrtu, *Int. J. Photoenergy* 2013, 1 (2013).
44. L.L. Estrella, M.P. Balanay, and D.H. Kim, *J. Phys. Chem. A* 122, 6328 (2018).
45. L. Huang, X. Sun, C. Li, R. Xu, J. Xu, Y. Du, Y. Wu, J. Ni, H. Cai, and J. Li, *Sol. Energy Mater. Sol. Cells* 157, 1038 (2016).
46. C. Wehrenfennig, G.E. Eperon, M.B. Johnston, H.J. Snaith, and L.M. Herz, *Adv. Mater.* 26, 1584 (2014).
47. T. Wang, J. Chen, G. Wu, and M. Li, *Sci. China Mater.* 59, 703 (2016).
48. L. Lin, L. Jiang, Y. Qiu, and Y. Yu, *Superlattices Microstruct.* 104, 167 (2017).